

See discussions, stats, and author profiles for this publication at: <https://www.researchgate.net/publication/303116699>

Thermo-mechanical and isothermal fatigue behavior of 316LN stainless steel with varying nitrogen content

Article in Metallurgical and Materials Transactions A · January 2015

CITATIONS

5

READS

98

6 authors, including:



Prasad Reddy G.V.

Indira Gandhi Centre for Atomic Research

90 PUBLICATIONS 788 CITATIONS

[SEE PROFILE](#)



Nagesha Atikukke

Indira Gandhi Centre for Atomic Research

110 PUBLICATIONS 1,027 CITATIONS

[SEE PROFILE](#)



R. Sandhya

Indira Gandhi Centre for Atomic Research

149 PUBLICATIONS 2,428 CITATIONS

[SEE PROFILE](#)



S. Sankaran

Indian Institute of Technology Madras

96 PUBLICATIONS 1,743 CITATIONS

[SEE PROFILE](#)

Some of the authors of this publication are also working on these related projects:



Vibration damping characteristics of epoxy based composites [View project](#)



High Strain Rate Deformation Study on Titanium alloys [View project](#)

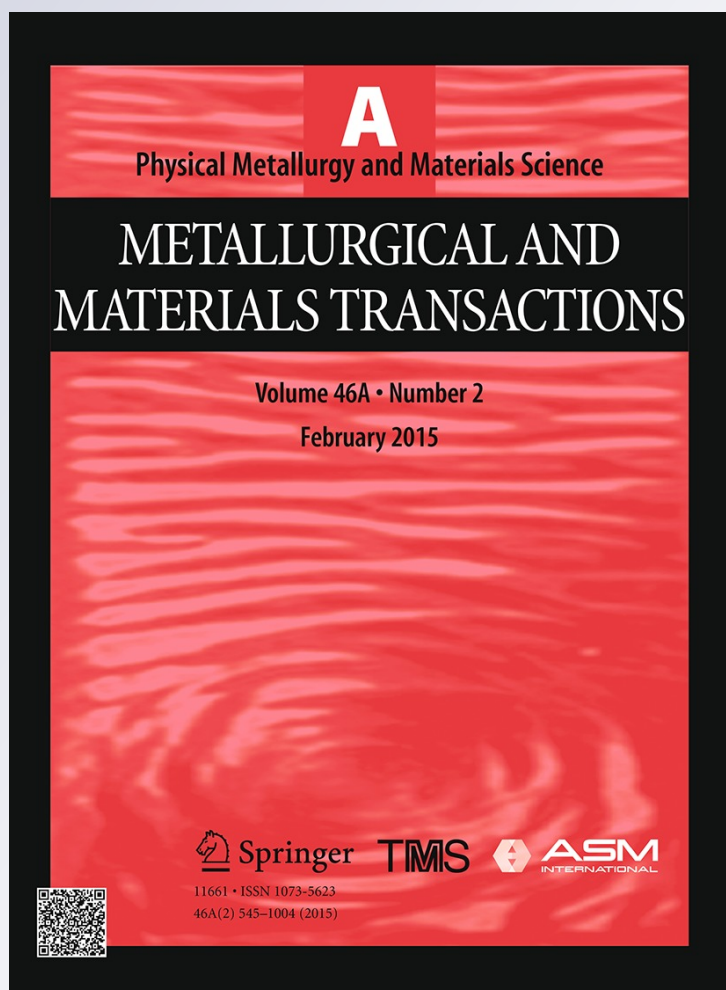
Thermomechanical and Isothermal Fatigue Behavior of 316LN Stainless Steel with Varying Nitrogen Content

**G. V. Prasad Reddy, A. Nagesha,
R. Sandhya, S. Sankaran, M. D. Mathew
& K. Bhanu Sankara Rao**

**Metallurgical and Materials
Transactions A**

ISSN 1073-5623
Volume 46
Number 2

Metall and Mat Trans A (2015)
46:695-707
DOI 10.1007/s11661-014-2653-y



Your article is protected by copyright and all rights are held exclusively by The Minerals, Metals & Materials Society and ASM International. This e-offprint is for personal use only and shall not be self-archived in electronic repositories. If you wish to self-archive your article, please use the accepted manuscript version for posting on your own website. You may further deposit the accepted manuscript version in any repository, provided it is only made publicly available 12 months after official publication or later and provided acknowledgement is given to the original source of publication and a link is inserted to the published article on Springer's website. The link must be accompanied by the following text: "The final publication is available at link.springer.com".

Thermomechanical and Isothermal Fatigue Behavior of 316LN Stainless Steel with Varying Nitrogen Content

G.V. PRASAD REDDY, A. NAGESHA, R. SANDHYA, S. SANKARAN,
M.D. MATHEW, and K. BHANU SANKARA RAO

Thermomechanical (TMF) and isothermal (IF) fatigue behavior of 316LN stainless steel alloyed with 0.07, 0.14, and 0.22 wt pct nitrogen is presented in this manuscript. In the TMF tests with temperature cycling in the range of 573 K to 873 K (300 °C to 600 °C), life decreased with increasing nitrogen content for both in-phase (IP) and out-of-phase (OP) cycling, with a peak at 0.07 wt pct N. In contrast, 0.14 wt pct N yielded maximum life under IF cycling carried out at 873 K (600 °C). Cyclic lives are seen to follow the sequence, IP-TMF < IF < OP-TMF cycling, and it remained same irrespective of the nitrogen content in 316LN SS. Lives under IP-TMF are lower than those in OP cycling by a factor of 2 to 2.5, in spite of the higher cyclic stress response in OP cycling. At all the nitrogen contents in the present study, nitrogen and dynamic strain aging induced slip localization in the form of planar slip bands both in IP and OP-TMF, in comparison to IF deformation wherein complete planar slip mode of deformation is evidenced only at 0.22 wt pct N. In TMF studies, increasing nitrogen content promoted strong slip localization (*i.e.*, increase in slip band density with a decrease in interband spacing) in combination with high tensile cyclic stresses that marred the beneficial effect of nitrogen content on TMF life.

DOI: 10.1007/s11661-014-2653-y

© The Minerals, Metals & Materials Society and ASM International 2014

I. INTRODUCTION

316LN stainless steel (SS) with 0.06 to 0.08 wt pct nitrogen constitutes a vital structural material for the primary side components (main vessel, inner vessel, intermediate heat exchanger, *etc.*) and piping system of Indian prototype fast breeder reactor (PFBR). These components are often subjected to cyclic thermal stresses as a result of reactor start-up/shutdown operations, thermal transients during normal operation, thermal stratification, *etc.*, in addition to the mechanical load variations. Moreover, the section thicknesses of some components reach up to 30 mm. From the viewpoint of cost and thermal stresses, it is necessary to reduce the section thickness which in turn demands the use of high-strength nitrogen-alloyed 316LN SS with increased resistance to high-temperature fatigue failure. Normally, design against fatigue failure under such

cyclic thermomechanical fatigue (TMF) loading is based on isothermal fatigue (IF) tests carried out at the peak temperature (T_{\max}) of the expected thermal cycle, which is assumed to lead to conservative life estimation. However, many engineering materials have been reported to display TMF lives inferior to IF lives, in contrast to the above design philosophy, due to temperature dependence of cyclic deformation and damage mechanisms in TMF.^[1–4] The present study is focused on the understanding of TMF deformation behavior of 316LN SS alloyed with varying nitrogen contents of 0.07, 0.14, and 0.22 wt pct, in comparison to IF tests conducted at the T_{\max} of TMF thermal cycle. The study also aims to identify the optimum nitrogen content for enhanced TMF life and to check the above design philosophy.

An increase in the nitrogen content in 316LN SS is reported to have beneficial influence on the fatigue life under IF cycling which is attributed to an increase in slip planarity and an associated increase in the slip reversibility.^[5] Optimum nitrogen content corresponding to the maximum life in IF tests has been reported to vary from 0.12 to 0.14 wt pct N.^[5–7] On the other hand, very limited literature is available on the TMF behavior of high nitrogen 316LN SS. Kim *et al.*^[8] have studied the influence of nitrogen on TMF life of 316LN SS alloyed with 0.02 and 0.1 wt pct N and reported a marginal increase in life with increase in nitrogen to 0.1 wt pct.

316LN SS is a planar slip material. Nitrogen addition to 316LN SS has been reported to induce cyclic softening at room temperature^[9,10] and is attributed to

G.V. PRASAD REDDY, Scientific Officer-E, A. NAGESHA, Scientific Officer-G, and R. SANDHYA, Head, Fatigue Studies Section, are with the Mechanical Metallurgy Division, Indira Gandhi Center for Atomic Research, Kalpakkam 603102, India. Contact e-mail: prasadreddy@igcar.gov.in; varprasad@gmail.com S. SANKARAN, Associate Professor, is with the Department of Metallurgical and Materials Engineering, Indian Institute of Technology Madras (IIT Madras), Chennai 600036 India. M.D. MATHEW, formerly with the Mechanical Metallurgy Division, Indira Gandhi Center for Atomic Research, is now Dean of Postgraduate and Research Studies with the Saintgits College of Engineering, Kottayam, Kerala, India. K. BHANU SANKARA RAO, Ministry of Steel Chair Professor, is with the Department of Metallurgical and Materials Engineering, Mahatma Gandhi Institute of Technology, Hyderabad 500075, India.

Manuscript submitted July 30, 2014.

Article published online November 20, 2014

a disordering of Cr-N short-range orders (SROs) in matrix.^[9] However, the extent of cyclic softening has been noticed to reduce at temperatures beyond 673 K (400 °C) where cyclic deformation is observed to be strongly influenced by dynamic strain aging (DSA) and/or secondary cyclic hardening, particularly for total strain amplitudes ≤ 0.6 pct; secondary cyclic hardening is noticed only for strain amplitudes less than 0.6 pct.^[10] DSA has been reported to induce localized planar slip and high matrix hardening (*i.e.*, increase in cyclic flow stress of the material) that drastically reduces the cyclic life in IF tests.^[11–13] The interplay between time and temperature-dependent processes (such as DSA, thermal recovery, creep, and oxidation) and their influence on the cyclic deformation and fatigue life are elucidated in this study, taking into account of the nitrogen content in 316LN SS. TMF tests, in the present study, were conducted over the temperature range of 573 K to 873 K (300 °C to 600 °C) that encompasses the temperature regime of interest [573 K to 823 K (300 °C to 550 °C)] to fast breeder reactors.

II. MATERIAL AND EXPERIMENTAL DETAILS

The chemical composition of the three heats of 316LN SS with 0.07, 0.14, and 0.22 wt pct N (henceforth designated as N07, N14, and N22, respectively) is given in Table I. A carbon content of about 0.03 wt pct was maintained in all the heats. The production details of the three heats are given elsewhere.^[10] Rectangular blanks of dimensions, 160 × 22 × 20 mm, were solution annealed at 1363 K (1090 °C) for 60 minutes followed by water quenching. Equiaxed grains free of delta-ferrite and precipitates were observed. The average grain sizes of the three heats, measured through mean lineal intercept method, were found to be in the range of $89 \pm 13 \mu\text{m}$. Tubular specimens with 1.5 mm wall thickness, 25 mm gage length, and 11.4 mm gage diameter (outer diameter) were used for both IF and TMF (in-phase (IP) and out-of-phase (OP)) tests. IP-TMF refers to the in-phase variation of temperature and strain simultaneously with respect to time, and accordingly the T_{max} of the thermal cycle coincides with the peak tensile strain. On the other hand, OP-TMF cycling imposes both temperature and strain waveforms together in out-of-phase condition such that the T_{max} coincides with the peak compressive strain. IP-TMF and OP-TMF tests were conducted at a fixed mechanical strain amplitude ($\Delta\epsilon_{\text{mech}}/2$) of ± 0.6 pct, with temperature cycling in between 573 K and 873 K (300 °C and 600 °C). The experimental setup, along with the procedure for the thermal compensation are elaborately described elsewhere.^[14] IF tests were conducted at the

above mechanical strain amplitude and at the T_{max} of TMF thermal cycle, *i.e.*, at 873 K (600 °C). A strain rate of $3 \times 10^{-5} \text{ s}^{-1}$ was employed for both the TMF and IF tests. The number of cycles corresponding to a 20 pct drop in the peak cyclic load was taken as the fatigue life. Transmission electron microscopy (TEM) studies were performed on thin foils prepared by twin-jet thinning using an electrolyte comprising 10 pct perchloric acid in methanol. The foils were examined with a 120 kV Philips CM12 microscope. Fractured surfaces of the failed samples were examined by scanning electron microscopy (SEM).

III. RESULTS AND DISCUSSION

In the following sections, cyclic deformation behavior under both TMF and IF conditions is described in terms of the cyclic stress evolution and stress-strain hysteresis loops. The probable hardening/softening mechanisms and substructural evolution are discussed. The inferences from the above, along with the fracture behavior, are then invoked to analyze the observed life variations between TMF and IF cycling, considering the influence of nitrogen content in 316LN SS.

A. Cyclic Deformation Behavior

The nature of cyclic stress response (CSR) observed under IF cycling is seen to be independent of the nitrogen content in 316LN SS, as depicted in Figures 1(a) through (c). All the three steels showed a CSR characterized by a brief initial cyclic hardening followed by a regime of cyclic saturation prior to a rapid stress drop marking the formation of macrocracks. In contrast to this, under OP-TMF cycling, only N22 steel exhibited the above CSR profile, while a gradual cyclic softening following an initial cyclic hardening is observed in N14 and N22 steels. In-phase TMF cycling, on the other hand, induced a continuous cyclic hardening followed by failure in N14 and N22 steels, and quasi-saturation before failure in the case of N07 steel (Figure 1(a)). Tensile stress amplitudes of the CSR curves under IP cycling [*i.e.*, IP(T)] are seen to be lower than those pertaining to OP cycling [*i.e.*, OP(T)], particularly for N14 and N22 steels (Figure 1). This is a consequence of the fact that the specimen traverses a regime of increasing temperature from 573 K (300 °C) at the peak compressive strain to 873 K (600 °C) at the peak tensile strain during the tensile ramp of IP-TMF cycling. The extent of initial cyclic hardening increased with increasing nitrogen content irrespective of the type of test, with the effect being more significant under IP cycling. In all the tests, nitrogen addition increased the

Table I. Chemical Composition (in Weight Percent) of Nitrogen-Alloyed 316LN Austenitic Stainless Steels

Designation	C	Cr	Ni	Mo	N	Mn	S	P
N07	0.03	17.5	12.2	2.49	0.07	1.7	0.0055	0.013
N14	0.03	17.5	12.1	2.53	0.14	1.74	0.0041	0.017
N22	0.03	17.5	12.3	2.54	0.22	1.7	0.0055	0.018

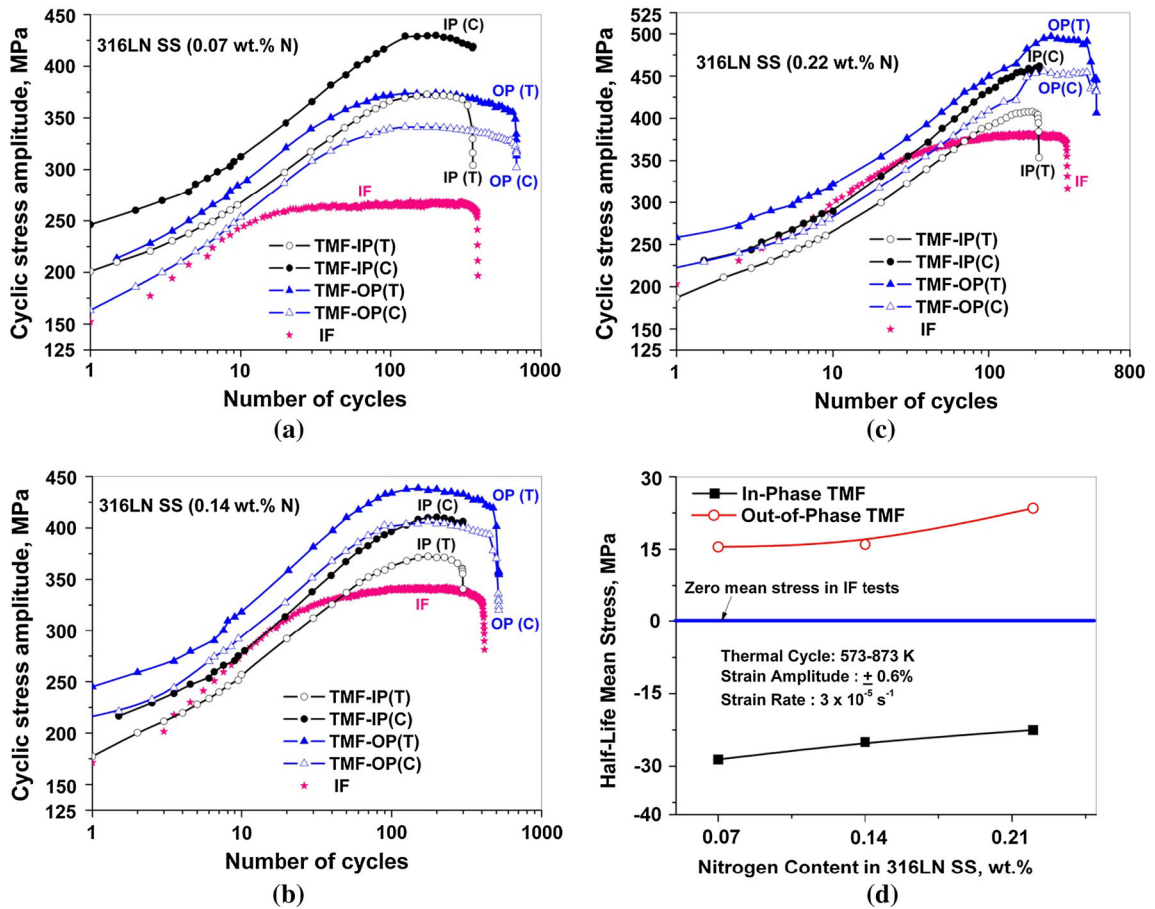


Fig. 1—(a through c) Cyclic stress response curves in TMF-IP, TMF-OP, and IF tests illustrating evolution of tensile (T) and compressive (C) stress amplitudes for (a) N07 steel, (b) N14 steel, (c) N22 steel; compressive stress amplitudes are shown in absolute values, and (d) Effect of nitrogen content on development of half-life mean stress in IP and OP tests. In figures (a through c), IP(T) and IP(C) refer to peak stress amplitudes in tension and compression, respectively, in IP cycling, and OP(T) and OP(C) also refer the same in OP cycling.

tensile stress amplitude of the CSR curve, as apparent from Figures 1(a) through (c).

The tensile and compressive stress responses obtained under IP and OP-TMF cycling are seen to be higher compared to those relevant to IF tests at the T_{max} of TMF cycle. This is because of the development of high deformation resistance during the low-temperature regime of TMF cycle, which partially offsets the reduction in flow stress at the subsequent high-temperature regime of the TMF cycle (where recovery processes such as climb and cross-slip could become significant). This in turn induces asymmetric cyclic stress evolution during tensile and compressive portions of the TMF cycle that leads to the development of tensile and compressive mean stresses under OP and IP cycling, respectively (Figure 1(d)). It may be noted that the mean stress under IF cycling is zero.

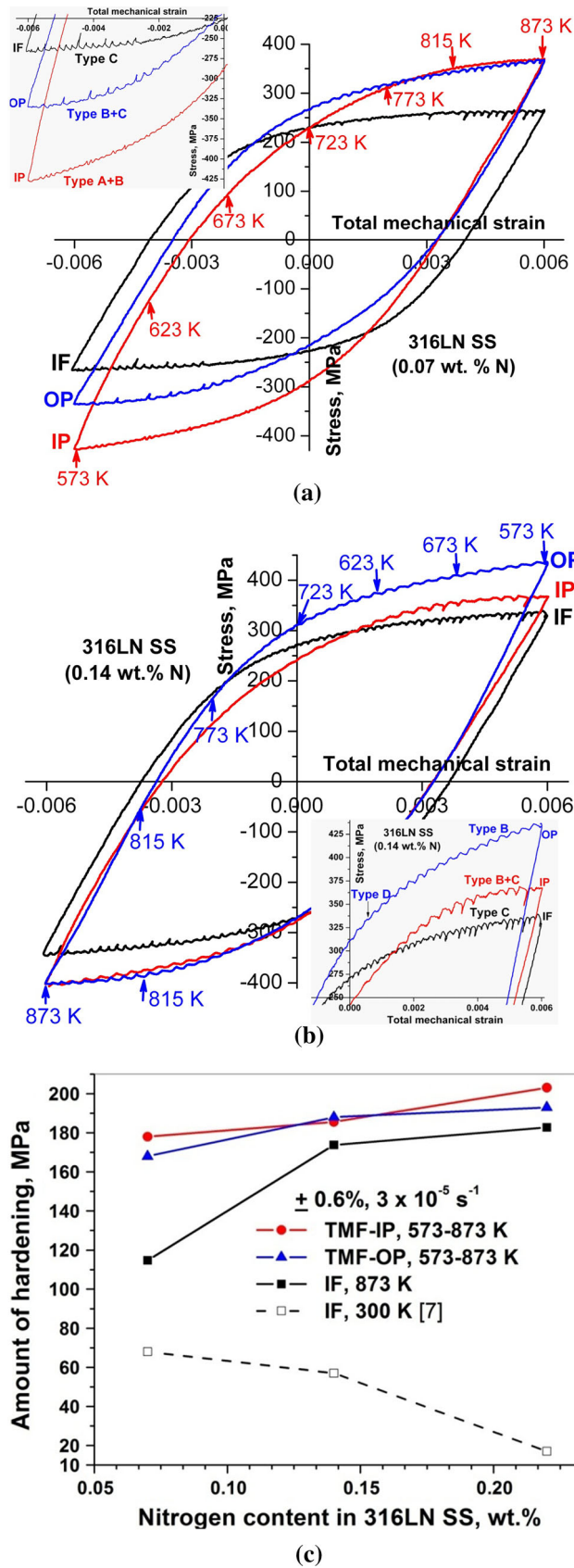
B. Phenomena/Factors Influencing the Cyclic Deformation Behavior

The cyclic stress response behavior during high-temperature fatigue is influenced, in general, by dislocation generation and their mutual interaction, dislocation-solute atom interactions (*i.e.*, DSA), recovery

processes (such as climb and cross-slip of dislocations), and creep. The occurrence of these mechanisms can be assessed partially from their characteristic manifestations in CSR curves, stress-strain hysteresis loops, deformation substructures, fracture surfaces, *etc.* It should be mentioned that TMF cycle incorporates within itself an additional cold work effect occurring during the low-temperature straining in successive cycles.

1. Dynamic strain aging

DSA results from attractive interaction between the solute species and mobile dislocations, either during their glide or temporary arrest at local obstacles in the glide plane. Consequently, in order to maintain an imposed strain rate, an increase in flow stress is mandatory either to unlock the dislocations from obstacles or to generate new dislocations. Two potential dislocation locking mechanisms, namely formation of Suzuki atmospheres of interstitial solutes in faulted areas of partial dislocations (leading to pronounced initial cyclic hardening) and the formation of Snoek atmospheres on dislocations (contributing to secondary cyclic hardening in the later stages of fatigue life) have been reported during DSA in 316L SS at 573 K



◀ Fig. 2—(a, b) Half-life stress strain hysteresis loops developed in IF, IP, and OP tests: (a) N07 steel and (b) N14 steel; insets show enlarged portion of serrations and (c) Comparison of amount of hardening incurred during DSA, between IF tests [at 873 K and 300 K (600 °C and 27 °C)] and TMF tests at the mechanical strain amplitude of ± 0.6 pct; In figures (a and b), the temperatures traversed during cyclic straining are indicated for an IP hysteresis loop in (a) and an OP loop in (b).

(300 °C).^[15,16] In strain controlled LCF deformation, DSA causes severe reduction in fatigue life which has been attributed to a reduction in the number of cycles to

crack initiation.^[11,13] In austenitic stainless steels, depending upon the applied strain rate (10^{-5} to 10^{-2} s^{-1}), DSA has been observed in the temperature range 473 K to 923 K (200 °C to 650 °C).^[17] Therefore, in the present study, DSA is expected to exert a marked influence on the deformation behavior and damage development in both the TMF and IF tests conducted at a strain rate of $3 \times 10^{-5} \text{ s}^{-1}$. Among the important manifestations pertinent to the occurrence of DSA,^[11–13] significant matrix hardening, prolonged period of initial cyclic hardening (Figures 1(a) through (c)) and serrations in hysteresis loops (Figures 2(a) through (b)) are noticed in the present study. As apparent from the distribution of serrations in TMF hysteresis loops, DSA persisted over the entire temperature range [573 K to 873 K (300 °C to 600 °C)] of TMF cycle, and hence influences the cyclic deformation to the maximum extent that resulted in, for example, a high degree of initial cyclic hardening as quantified in Figure 2(c). Figure 2(c) shows the amount of cyclic hardening incurred during DSA in the present tests, at a cumulative strain of 1.2 (corresponding to first 100 cycles), along with the amount of hardening in IF test at room temperature (at 0.6 pct strain amplitude and $3 \times 10^{-3} \text{ s}^{-1}$ strain rate) where DSA is absent. In Figure 2(c), the initial cyclic hardening experienced by the material is quantified in terms of amount of the increase in stress amplitude from 1st to 100th cycle. The amount of stress increase is calculated as $((\Delta\sigma/2)_{100} - (\Delta\sigma/2)_1)$ i.e., the difference between half of first cycle stress range $(\Delta\sigma/2)_1$ and half of stress range corresponding to the 100th cycle $(\Delta\sigma/2)_{100}$; at 300 K (27 °C) (and at a strain rate of $3 \times 10^{-3} \text{ s}^{-1}$), all the steels showed considerable cyclic softening beyond 20 cycles,^[10] and hence the amount of hardening is calculated up to 20 cycles. Significant hardening induced during DSA under IP and OP cycling can be noticed from Figure 2(c), and it is also observed that the initial cyclic hardening increased with increasing nitrogen content. In the case of IF tests at 873 K (600 °C), the amount of hardening is observed to be lower than that recorded in TMF (Figures 1(a) through (c) and 2(c)), due to constant temperature throughout the IF cycling. Furthermore, the cyclic hardening observed under IF and TMF are vastly different. While the hardening phase lasted only about 20 to 30 cycles under IF cycling, it is seen to extend to about 100 cycles under TMF. This could be due to the differences in occurrence of DSA during the tensile and compression halves of the cycle and has not been analyzed in the present study. In a recent study on 316L SS, Pham *et al.*^[15] attempted an investigation in this direction and reported the differences in striations in tensile and compression halves of the hysteresis loops. The above authors have attributed it to the influence of hydrostatic

pressure on the vacancy mobility which is found to be enhanced during tensile direction transients and suppressed during the compressive direction transients.

Regarding the type of serrations, Type-A, Type-B, Type-C, and Type-D serrations are noticed in IP and OP-TMF depending on the nitrogen content, while Type-C serrations are observed in the IF tests irrespective of the nitrogen content. Type-A serrations characterize the stress rise followed by a stress drop to below the general stress–strain curve, whereas Type-B serrations fluctuate about the stress–strain curve.^[18] Both are considered as ‘locking serrations.’ Type-C serrations show stress drops below the general stress–strain curve and are generally attributed to the unlocking of dislocations from the already existing atmospheres of solute atoms.^[18] Type-D serrations appear as ascending steps over and above the general level of stress strain curve, and they occur alone or with Type-B serrations.^[19] Usually Type-B, Type-C, and Type-D serrations form at low strain rates, while Type-A serrations appear in the low-temperature part of the DSA regime.^[18,19]

2. Recovery processes and creep

Recovery processes, *i.e.*, thermally activated dislocation motion by climb and cross-slip, become significant at temperatures ≥ 823 K (550 °C) in austenitic stainless steels which tend to reduce the flow stress.^[20] However, simultaneous occurrence of DSA, as observed in the present study, partially suppressed such recovery as the former (*i.e.*, DSA) is known to promote planar slip that constrains the dislocation motion to planar glide. Hence, the magnitude of flow stress at any given strain in a hysteresis loop is the resultant of a synergistic interaction between the recovery processes and DSA. Although the same is true for IF tests, due to the constant test temperature throughout the cycling, recovery processes tend to dominate and counterbalance the hardening effect brought about by DSA, in turn causing a significant reduction in the CSR in comparison to that observed in TMF (Figures 1(a) through (c)). The entire test temperature range employed for TMF in the present study lies within the temperature domain of the occurrence of DSA (as apparent from the serrations in Figures 2(a) and (b)), as result of which the cyclic hardening effect effectively outweighs the softening brought about by the recovery processes. The cyclic hardening effect is, however, found to be strongly influenced by nitrogen content in 316LN SS, in both TMF and IF tests. As is evident from Figures 1(a) through (c) and 2(c), nitrogen addition beyond 0.07 wt pct considerably enhanced matrix hardening probably by counteracting the recovery processes to a larger extent. This is also found to be associated with a change in the slip mode with increasing nitrogen content, as would be dealt with, in the later part of the text (Section III–C).

In Type 316 SS or its variants, it is reported that creep deformation (by dislocation climb) becomes significant at temperatures ≥ 823 K (550 °C).^[21] Zauter *et al.*^[22] have reported stress relaxation (associated with creep deformation) in hysteresis loop before reaching the maximum strain under IP cycling in 304 SS with

$T_{\max} \geq 923$ K (650 °C). In the present study, however, the peak stress coincided with the peak applied strain, and there is no stress relaxation in hysteresis loops (of IP and OP, Figures 2(a) and (b)); it may be noted here that the total data points collected per cycle (or one hysteresis loop) in the current study is 3199 points (~4 data points/second) which is sufficient to capture the minute changes in curvature of the hysteresis loop. This, however, does not rule out the occurrence of creep in the present study, as matrix hardening due to DSA can offset the stress relaxation. Indeed, microscopic unbalanced grain boundary sliding displacements (while creeping) develop during TMF cycle that manifest in the form of intergranular cracks.^[1,23] In the current study also, fracture surfaces under IP and IF cycling revealed intergranular cracking which is discussed in Section III–D with reference to creep, oxidation, and slip band grain boundary intersections.

From the above observations, it can be inferred that a competition between DSA and recovery processes dictates the cyclic deformation behavior in both IF and TMF tests (Figure 1). While the former dominates in TMF cycling, the latter gains significance under IF deformation.

C. Deformation Microstructural Changes

1. Dislocation substructural evolution

Dislocation substructures associated with cyclic deformation, in the present study, are found to depend both on the nitrogen content in 316LN SS and the type of fatigue test. The dependency is seen to affect the slip mode of deformation and the extent of occurrence of planar/wavy/mixed slip mode.

In N07 steel subjected to IF cycling at 873 K (600 °C), dislocation cell structures (mainly equiaxed) are noticed (Figure 3(a)). In addition, the formation of elongated cells from dislocation walls is evidenced by the presence of arrays of dislocations in the deformation zone between the walls (Figure 3(b)). Although DSA is present, recovery processes that predominate at 873 K (600 °C) could have reconfigured the dislocation structure into dislocation cells and walls in N07 steel. In the case of N14 steel that contains twice as much nitrogen (0.14 wt pct), slip bands with high dislocation activity (Figure 3(c)) impinging on grain boundaries are frequently observed. In addition, dislocation cells (equiaxed and elongated) are noticed in few grains (Figure 3(d)). With further increase in nitrogen content to 0.22 wt pct, cyclic plastic strain is mostly seen to be accommodated by planar slip bands (Figure 3(e)). From these observations, it can be concluded that a change in nitrogen content altered the slip mode from wavy in N07 steel to predominantly planar slip mode in N22 steel. Further, it can be inferred that strain hardening resulting from DSA (in addition to that caused by dislocation–dislocation interactions) together with an increase in tendency to planar slip (by DSA and interstitial nitrogen) with increasing nitrogen content caused an increase in CSR with nitrogen (Figures 1(a) through (c)), by compensating the softening effect due to thermal recovery.

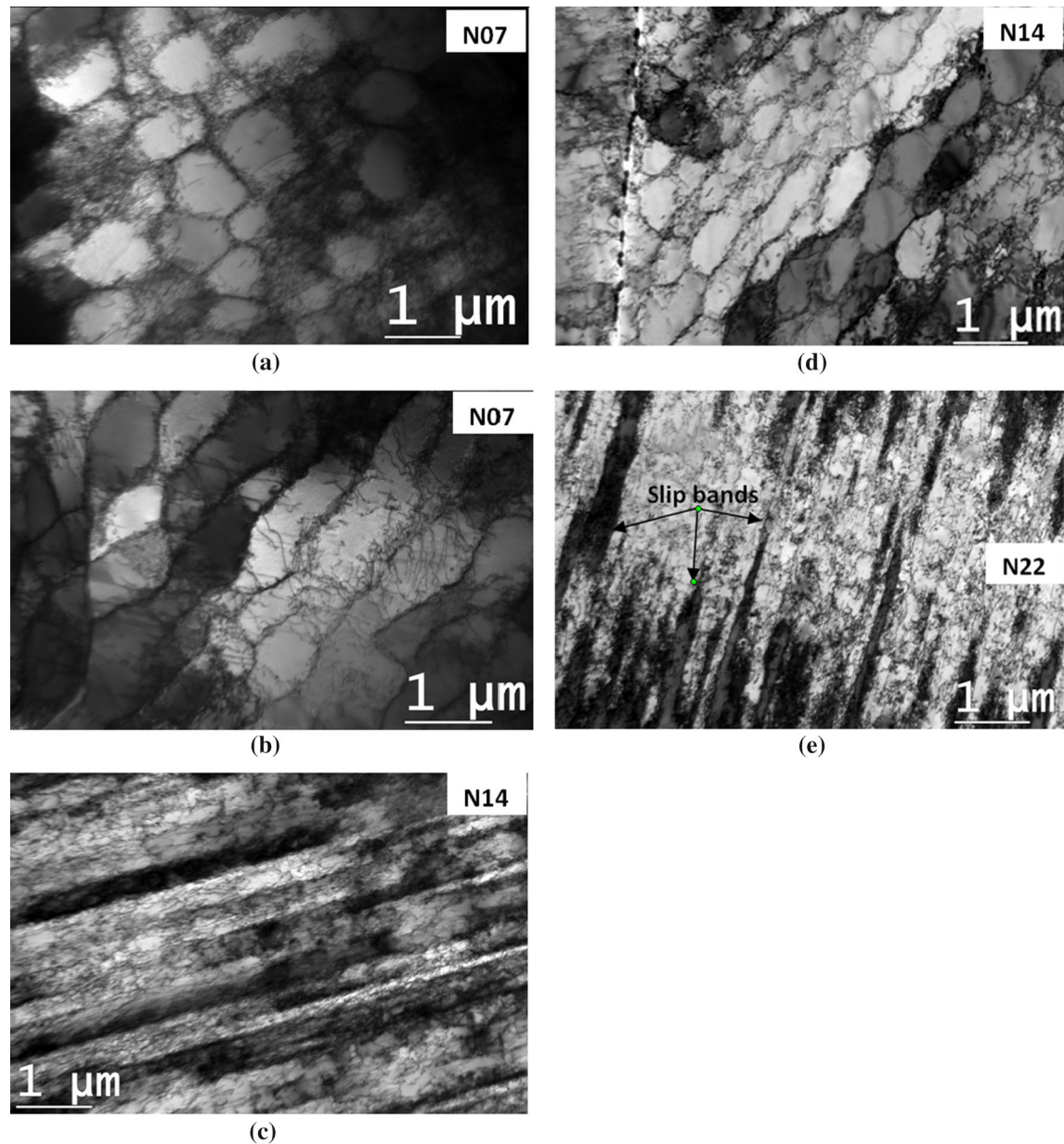


Fig. 3—Bright-field TEM images of dislocation substructures developed during isothermal fatigue deformation, as a function of nitrogen content in 316LN SS at 0.6 pct total strain amplitude, (a, b) N07 steel, (c, d) N14 steel, and (e) N22 steel.

In contrast to IF, cyclic deformation in IP and OP-TMF is accomplished mainly by planar slip mode in all the steels (Figure 4), since DSA is observed to control the TMF deformation as discussed above (Section III-B). As DSA promotes planar slip, in addition to that caused by nitrogen, dislocation motion is constrained to glide motion, and thus planar slip bands are noticed in IP and OP test conditions. In IP-TMF, an increase in the slip band density, together with a decrease in the interband spacing, is observed with increasing nitrogen content, resulting in an extensive planar slip in N22 steel (Figures 4(a) through (c)). OP cycling too showed a similar substructural evolution with nitrogen. It may, however, be noted that the severity of planar slip reduced under OP in comparison to IP cycling, as

reflected by the presence of more widely spaced slip bands (Figures 4(d) through (f)). This indicates possible dissimilarities in the planar mode of deformation between the two cycling conditions. The reason for the above dissimilarity is not clear from the present studies, and further investigations are needed to explain the observed substructural differences in IP and OP.

Apart from the above observed dislocation structures, it is important to mention that in 316L SS, corduroy structure (constituting small faulted dislocation loops mainly of vacancy type and/or cavities aligned along certain orientations in localized deformation bands) has been reported in IF tests conducted at intermediate temperatures [473 K to 773 K (200 °C to 500 °C)] and at low total strain amplitudes (e.g. ± 0.25 and

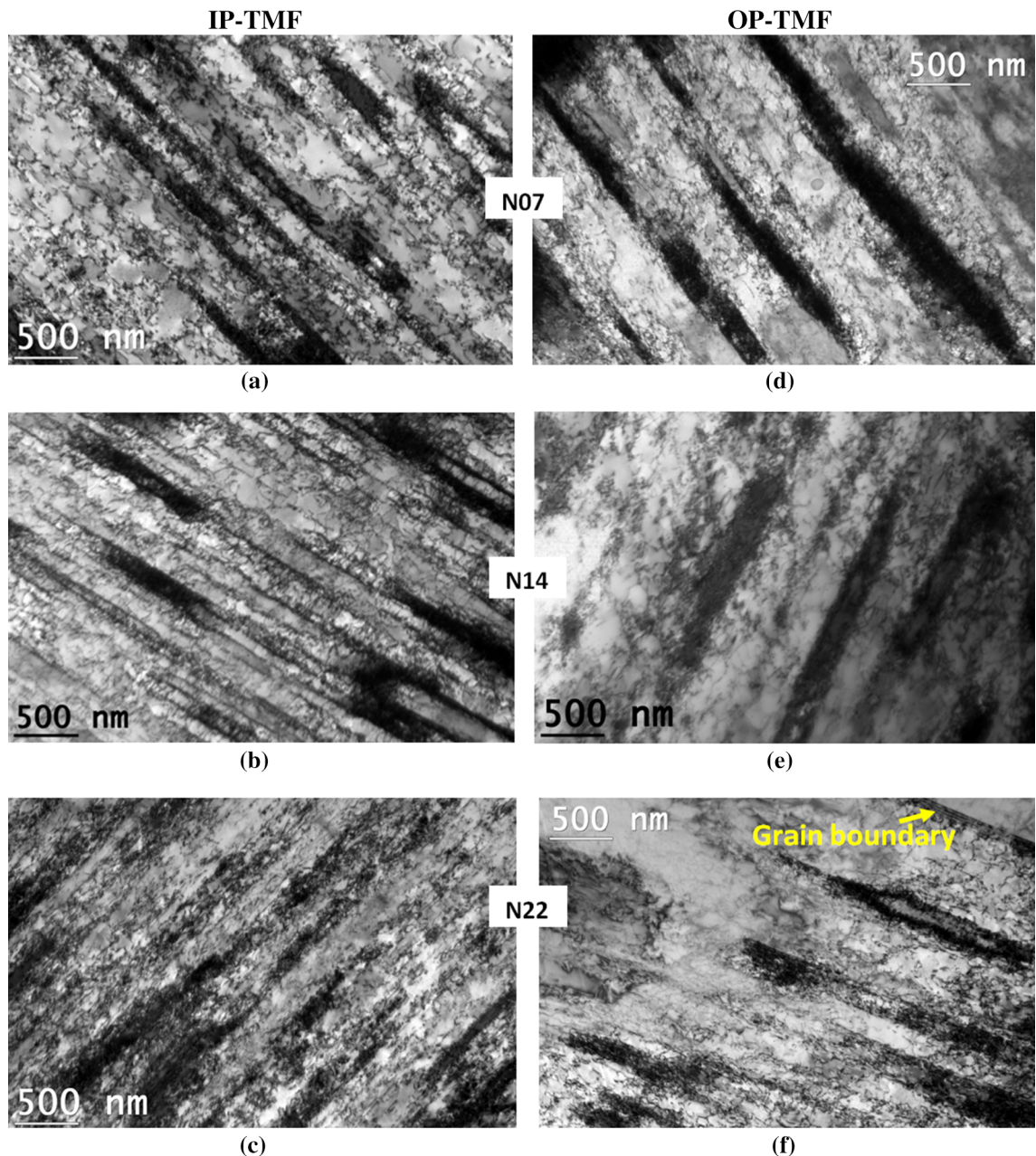


Fig. 4—Bright-field TEM images of dislocation substructures developed during IP and OP-TMF deformation, as a function of nitrogen content in 316LN SS at 0.6 pct mechanical strain amplitude, (a through c): IP-TMF and (d through f): OP-TMF.

0.4 pct).^[15,16,24,25] In 316L SS, occurrence of corduroy structure has been shown for the first time in air environment, and the origin of formation of corduroy structure and its variants and the need for excess vacancy concentration has been elucidated in detail by Pham *et al.*^[15,16] The above observations are noticed in the temperature regime of occurrence of DSA. These studies, however, suggest a strong dependence on the combination of applied strain amplitude, test temperature, and environment for the formation of corduroy structure. Moreover, it is also emphasized that the formation of corduroy structure occurs after a certain number of

cycles^[15,16,24,25] or toward the end of the life.^[15,16] In the present study, low applied strain rate, high test temperatures above 773 K (500 °C) in IF and TMF, high total strain amplitude (± 0.6 pct), and the observed low number of cycles to failure (in comparison to that in References 15, 16, 24, 25) could have altogether lowered the vacancy concentration below that required for the formation of corduroy structure. Hence, the corduroy structure is not evidenced in the present study. In fact, in 316L SS, corduroy structure has not been predominantly observed for the LCF tests at 573 K (300 °C) and at total strain amplitude of 0.7 pct.^[15,16]

2. Cyclic strain-induced precipitation

In AISI type 316 SS, the generally observed second-phase constituents that form upon elevated temperature exposure are $M_{23}C_6$ and M_6C carbides, and other intermetallic phases such as chi, laves, and sigma phase. However, precipitation of chi and laves phases requires substantial amounts of Mo or Nb or Ti contents^[26]; for example, chi phase contains Mo in the range of 18-26 wt pct, whereas laves phase contains about 45 pct Mo.^[26] M_6C carbide is a minor phase and is prominent in Mo-containing stainless steels. $M_{23}C_6$ is the major carbide precipitate in Fe-Cr-Ni steels, Cr being its main metallic constituent. The solubility of carbon in 316 SS at 873 K (600 °C) has been found to be about 4 ppm only,^[27] and consequently $M_{23}C_6$ (M = Cr, Fe, Mo, Ni) carbide is generally the first phase to form in austenitic stainless steels.^[28]

It has been reported that precipitation of carbides ($M_{23}C_6$ and M_6C) in 316L SS requires about 50 hours of thermal aging at 873 K (600 °C).^[29] Also, nitrogen addition to 316L SS is reported to delay the onset of carbide precipitation.^[30] In contrast to these observations, $M_{23}C_6$ carbide precipitates are observed in the present study irrespective of the nitrogen content. These carbides with high chromium content are observed to

form along the grain boundaries, as shown in Figures 5(a) through (f), and are noticed in all the tested samples. Diffraction analysis of the precipitate is shown in Figure 5(g). In comparison to IF-tested samples, TMF deformed samples have shown a considerable reduction in the density of carbides particularly in N07 (Figures 5(a) and (d)) and N14 steels (Figures 5(b) and (e)); comparison is shown for OP and IF-tested samples only. OP and IP-TMF tested samples have shown more or less the equal extent of precipitation irrespective of nitrogen content, as shown in Figures 5(c) and (f) (for N22 steel only).

The precipitation of di-chromium nitride (Cr_2N) is expected in nitrogen-containing austenitic steels upon high-temperature exposure. Formation of Cr_2N precipitate has been reported at temperatures above 873 K (600 °C),^[31] and moreover precipitation has been observed in alloys containing greater than 0.1 wt pct N^[32] in Fe-Cr-Ni or Fe-Cr-Mn austenitic stainless steels. However, in the present study, even at a nitrogen content of 0.22 wt pct N, Cr_2N is not observed in the deformed samples, and it could be due to the following two reasons:

- (i) Cr_2N precipitation sequence, on thermal aging, has been elucidated in detail by Shankar *et al.*^[33] and is

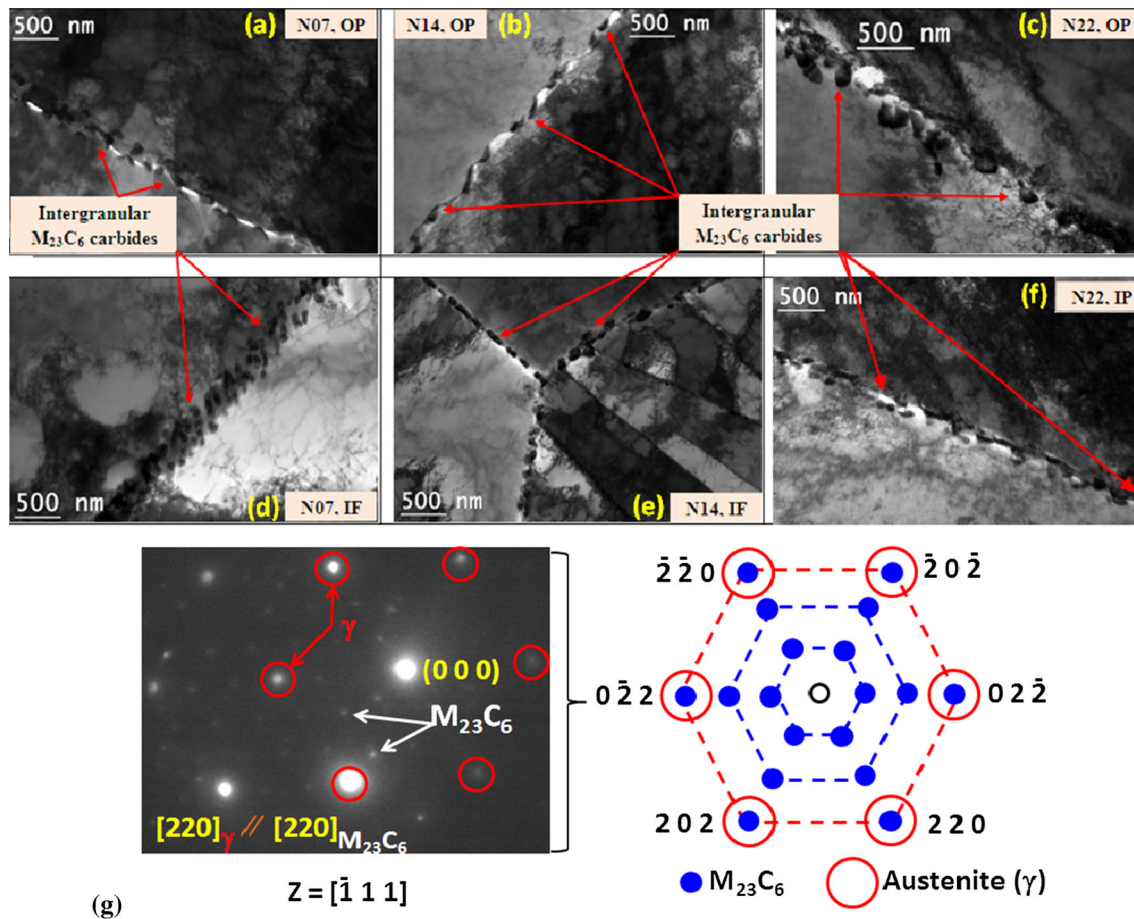


Fig. 5—TEM images of cyclic deformation induced intergranular $M_{23}C_6$ carbides in, (a through c) OP-TMF tests: (a) N07 steel, (b) N14 steel, (c) N22 steel; (d, e) IF tests at 873 K (600 °C): (d) N07 steel, (e) N14 steel, (f) IP-TMF tested N22 steel, and (g) Diffraction pattern and indexing of $M_{23}C_6$ carbide and matrix, along with the orientation relationship between them and zone axis (Z).

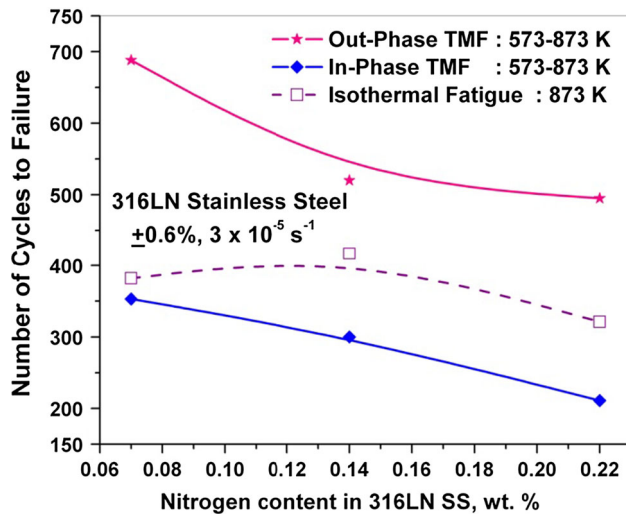


Fig. 6—Influence of IP, OP, and IF cycling on fatigue life as a function of nitrogen content in 316LN SS.

given as supersaturated solid solution (fcc) → formation of Cr-N complexes (fcc) → intragranular Cr₂N precipitates (hcp) → Cr₂N cellular precipitation (hcp). Since LCF deformation destroys the ordering of Cr-N complexes during the to and fro motion of dislocations,^[9] formation of Cr₂N could have been suppressed.

- (ii) In addition, precipitation of M₂₃C₆ carbides could have reduced the concentration of Cr required for the formation of Cr₂N; it requires about 88 pct Cr and 11.8 pct of N for the Cr₂N formation.

Since intragranular precipitation of fine size is not significantly evidenced in the present study, contribution to cyclic hardening is negligible from the aforementioned precipitation. The important consequence of precipitation thus includes removal of solid solution strengthening elements from the matrix that could decrease the matrix strength, in addition to that caused by the recovery processes.

D. Fatigue Life and Fracture Behavior

TMF life decreased with an increase in nitrogen content under both IP and OP-TMF cycling with a maximum in life at 0.07 wt pct N (Figure 6). However, under IF cycling, a peak in life is noticed at a nitrogen content of 0.14 wt pct N. OP-TMF lives (N_{OP}) are observed to be higher than those in IP case (N_{IP}) by a factor of 2 to 2.5, notwithstanding the higher cyclic tensile stress associated with the former. Fatigue lives under IF cycling (N_{IF}) at 873 K (600 °C) are seen to lie in between those of IP and OP-TMF. Cyclic lives are thus seen to follow the sequence, IP-TMF < IF < OP-TMF cycling, and it remained same irrespective of the nitrogen content in 316LN SS. The relative roles of deformation mechanisms and fracture mode on the observed fatigue lives are discussed below. In comparison to the life sequence observed in the present study, there have been several studies on 316L/304L SS that

reported variations in the life sequence (IF < IP < OP,^[1,14] IP < IF < OP,^[2] OP < IP < IF,^[3] to name a few), depending on the applied temperature range and strain range in TMF tests.

1. Comparison of IP and OP-TMF lives with IF lives

The fracture surfaces of the failed samples are analyzed through SEM fractography. Selected images pertaining to the different testing conditions and nitrogen levels are presented in Figures 7(a) through (f). As is apparent from the above fractographs, fracture surfaces of IF (Figures 7(a) through (c)) and IP (Figures 7(d) through (f)) tested samples revealed predominantly intergranular cracking, while OP cycling induced transgranular crack propagation (Figures 8(a) and (b)). Previous investigations have ascribed such intergranular cracking in IP and IF tests either to creep damage or grain boundary oxidation or both.^[1,14,34] In order for the creep deformation to assume significance, tensile creep condition should exist in the test conditions as it is more amenable to cavity or wedge-crack nucleation in austenitic stainless steels, provided that the test temperatures are above $0.45T_m$ [i.e., 815 K (542 °C)] and strain rates are $<10^{-5} \text{ s}^{-1}$, where T_m is the melting point in Kelvin. Usually low stress and long-range diffusion are mandatory for the nucleation of cavities on grain boundaries (perpendicular to load axis), and this requires very low strain rates in comparison with the present test conditions. On the other hand, creep fractures under high stress and intermediate-to-high temperature conditions, such as in the present study [in the temperature range of 815 K to 873 K (542 °C to 600 °C)], generally involve wedge cracking at grain boundary triple point junctions. Triple point cracks nucleate by grain boundary sliding which can occur either by diffusion process or by stress gradients near the grain boundaries brought about by slip band impingements on the grain boundaries.^[35–37] It has been suggested that slip band impingements on the grain boundary during DSA generate large internal stresses which are believed to drive grain boundary sliding at a sufficiently high rate.^[35] Since the stress produced by grain boundary sliding at triple point hardly relaxes due to the already hardened matrix (because of DSA), crack nucleates at grain boundary triple points. Intergranular fracture due to triple point cracks has been reported to result from the hardening of matrix due to strain aging during creep at high stresses below 823 K (550 °C).^[38] For the present test conditions in IP-TMF, tensile creep deformation could be expected to occur in the temperature range of 815 K to 873 K (542 °C to 600 °C) but over a period of 78 seconds in every cycle. On the other hand, in IF cycling at 873 K (600 °C), tensile creep damage accumulates over a period of 400 seconds (during the tensile ramp of every cycle) which could get partially healed by beneficial compressive creep over the same period during the compression ramp.^[39] In the case of IF-tested samples, the grain boundary sliding could be attributed to result from both diffusional processes and slip band impingements on grain boundary, whereas in the case of IP-TMF where the deformation mode is strongly planar, it is likely that slip band

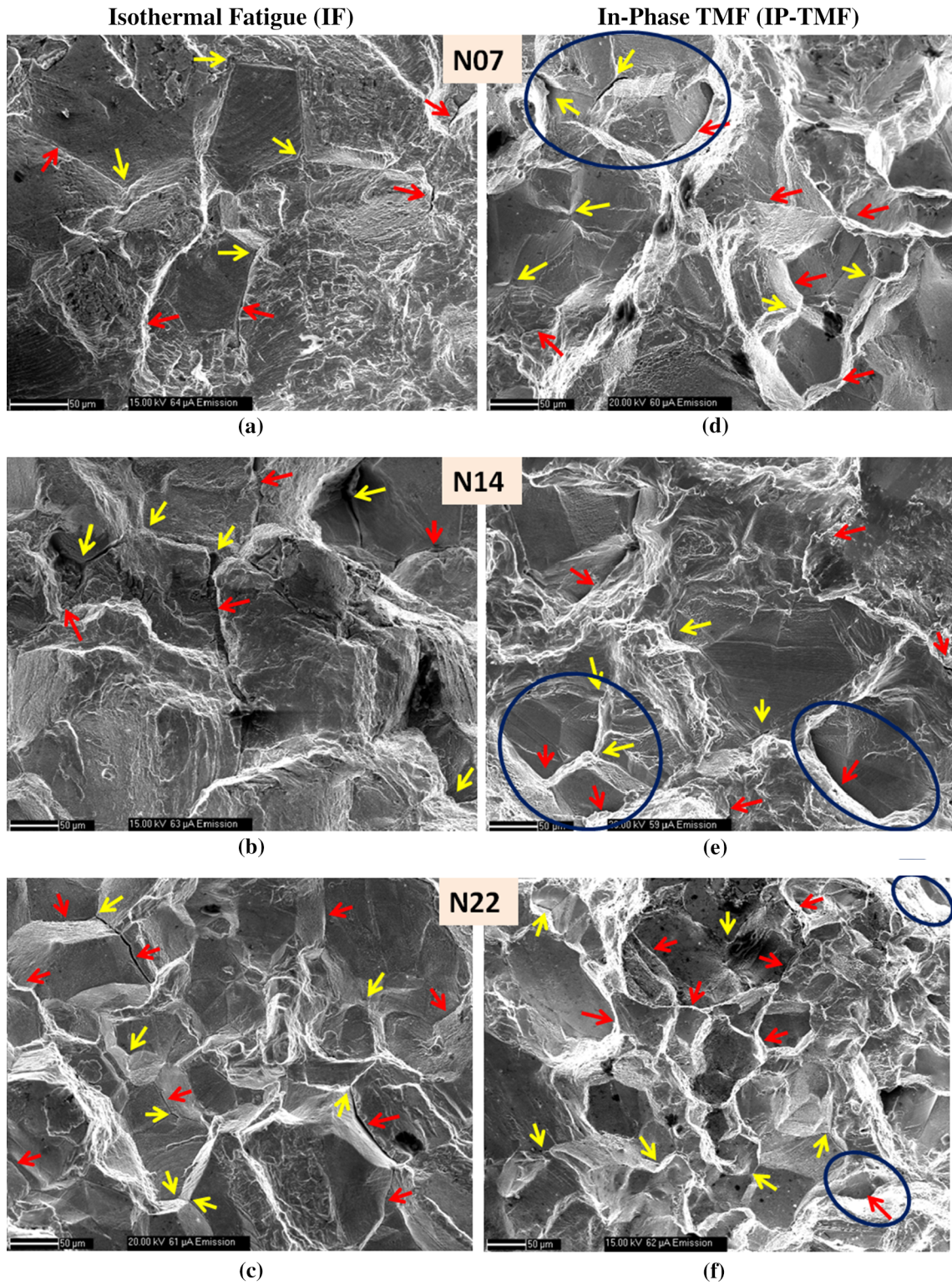


Fig. 7—SEM fractographs illustrating predominantly intergranular fracture in (a through c) IF and (d through f) IP-TMF tested samples; triple point cracks and grain boundary decohesion are marked by arrows.

impingements play a major role on the dynamics of grain boundary sliding. The detrimental influence of IP-TMF and IF cycling can be noticed from the large fraction of triple point cracks and grain boundary

decohesions on fractographs of IP and IF-tested samples (Figures 7(a) through (f)). On the other hand, in OP-TMF, the temperatures traversed during the tensile half of cyclic deformation are not enough to cause

Out-of-Phase TMF (OP-TMF)

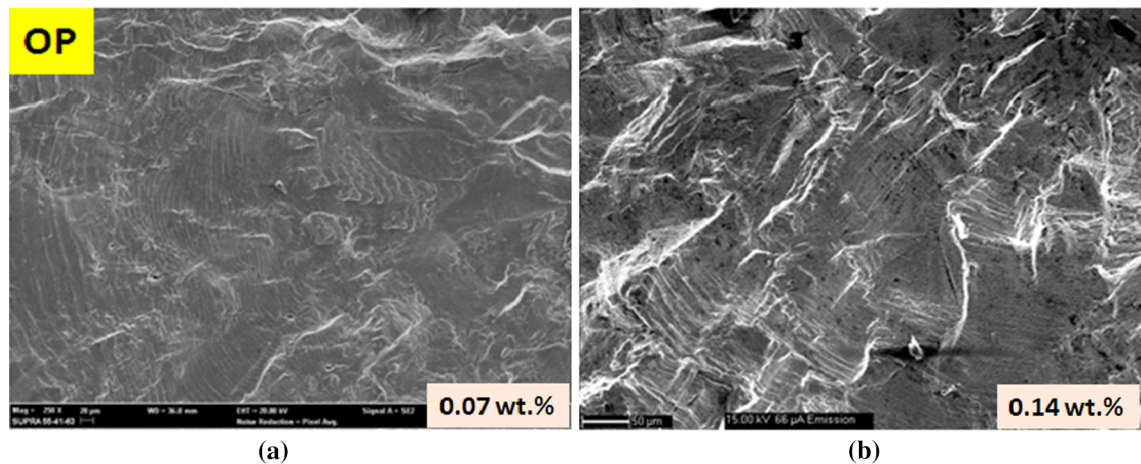


Fig. 8—SEM fractographs of OP-TMF tested samples illustrating transgranular fracture under OP-TMF cycling in (a) N07 steel and (b) N14 steel.

weakening of the grain boundaries. Moreover, compression creep occurring either under OP cycling (*i.e.*, during compression half of hysteresis loop) or compression hold conditions is found to be less harmful, as it inhibits creep cavities or even partially heals out the previously nucleated cavities/cracks.^[1,23,40,41] In fact, in 304L SS, based on the measurements of grain boundary sliding displacement (taken from the scribed surfaces of tested specimens), Fujino *et al.*^[1] have reported significant accumulation of grain boundary sliding displacements in in-phase TMF tested specimens, compared to negligible residual sliding displacement in out-of-phase TMF and IF-tested samples. On similar grounds, Ellison and Paterson *et al.*^[40] have found that small amount of compression hold (for *e.g.*, 30 minutes tension hold plus 3 minutes compression hold) in a cycle is found to effectively reduce the internal grain boundary cracking and lead to prolonged life. Hence, the deformation and damage in OP cycling develops mostly within the grains and can be evidenced by the transgranular crack propagation (*i.e.*, striations) in OP-TMF tested specimens (Figures 8(a) and (b)).

As evident from the fractographs (Figures 7(a) through (f)), oxidation is present in all the tested samples, irrespective of the nitrogen content, especially under IP-TMF and IF cycling conditions. In IP cycling, oxidation occurs mainly during tensile half of the cycle which allows an easy ingress of oxygen to the crack surfaces/tips, in turn hastening the intergranular damage. It is important to mention that OP-TMF is particularly detrimental for materials that are prone to oxidation such as carbon steels and Cr-Mo steels, in which OP lives have been reported to be lower than those noticed in IP.^[1,34,42] It may be noted that under OP cycling, the oxide that forms during the compression half of the cycle is subjected to tensile strain as the temperature reverses to low-temperature part of the cycle. This, coupled with the tensile mean stress, causes the oxide scale to crack owing to its low ductility at low temperatures, in oxidation-prone steels. This, however,

could not significantly influence the OP-TMF lives in the present study.

The above observations justify higher life in OP cycling, since intergranular cracking due to creep and oxidation damages is negligible because of the out-of-phase relationship between the high temperatures and the tensile deformation. In contrast, predominant intergranular cracking in IF and IP-TMF tested samples partly bypasses lattice resistance and grain boundary barrier effect to the propagating crack front, that could accentuate the crack propagation rate, which in turn caused inferior fatigue lives in IF and IP-TMF. The damaging influence of IP-TMF cycling (with and without tensile hold periods) has also been reported to result in lower lives than those observed in OP cycling, in austenitic stainless steels.^[1,23]

2. Reasons for the lower IP-TMF lives compared to IF lives

Periodic exposure to high temperatures during tensile ramps in IP-TMF cycling would be generally expected to decrease the tendency toward oxidation and creep-induced intergranular cracking, and thereby enhance the fatigue lives in comparison to IF cycling. In contrast to this, IP-TMF cycling is found to cause lowest lives, at all the nitrogen contents in 316LN SS, below those obtained under IF cycling as apparent from Figure 6. Also, fractographs of samples tested under IP-TMF showed more or less similar intergranular damage as that observed under IF cycling (Figures 7(a) through (f)). One interesting feature observed on the IP fractographs has been the presence of overgrown cavity/crack sites (marked in circles in Figures 7(d) through (f)). These observations signify the deleterious influence of IP cycling also, which could be responsible for the reduction in life compared to that of IF-tested samples. There are two possibilities for this to take place:

(a) Growth and accumulation of intergranular damage depends on the tensile stress. The comparative

CSR behavior between TMF and IF cycling shown in Figures 1(a) through (c) indicates that the tensile stresses in IP-TMF are considerably higher than those in IF cycling for all the nitrogen contents. This in turn implies that the propagation of intergranular damage in IP cycling takes place at much higher tensile stresses compared to the IF cycling which would accelerate the crack growth rates in IP compared to IF, in spite of the mean compressive stresses in IP cycling. The higher tensile stress could also mean a larger crack tip/mouth opening under IP-TMF, contributing to an enhanced crack tip oxidation, in comparison with IF cycling. It is important to mention that only tensile creep conditions prevail in IP-TMF, since the compressive deformation taking place at lower temperatures offers no scope for any damage reversal (unlike in IF cycling).

- (b) In addition to the above, it is also important to analyze and establish the role of substructural development (Figures 3 and 4(a) through (c)) on intergranular damage. As apparent from these figures, localization of dislocation slip is seen to manifest in the form of planar slip bands under both IF (exception being N07 steel) and IP cycling, with some instances of their impingement on the grain boundary; in the case of N14 steel tested under IF cycling, mixed mode of deformation is observed as shown in Figures 3(c) and (d). Slip localization is noticed to be very strong and spread over a larger area in IP tested samples, in comparison to IF. This can cause stress concentration at points of intersection of grain boundary and slip band, thereby enhancing the tendency toward intergranular wedge cracking (as mentioned in Section III–D–1). Slip band impingement on grain boundary with or without precipitates has been reported to be highly deleterious from the viewpoints of early crack initiation and rapid crack coalescence that accentuate crack propagation.^[43] The detrimental influence of strong strain localization is partly responsible for the reduction in life observed under IP-TMF cycling.

3. Effect of nitrogen content on TMF life under OP and IP cycling

Nitrogen is beneficial with respect to creep, as creep strength has been reported to increase in 316LN SS with increasing nitrogen content which is attributed to a reduction in the density of intergranular cavitated sites.^[44] In spite of this, both IP and OP cycling induced reduction in TMF life with increasing nitrogen content. The influence of nitrogen content on oxidation could be minimal, as fractographs of all IP-TMF (or OP-TMF) tested samples showed more or less similar degree of oxidation irrespective of nitrogen content.

From the deformation substructures in IP and OP (Figure 4), it can be noticed that planar slip prevailed, rather than wavy slip, under both the test conditions due to DSA and nitrogen content in 316LN SS, both of which impede the cross-slip of dislocations. Increase in

nitrogen content is found to enhance the slip localization with a concomitant increase in slip band density coupled with a decrease in the interband spacing. This, in combination with high tensile stresses at high nitrogen contents (Figures 1(a) through (c)), could have led to rapid crack nucleation and coalescence, ultimately bringing down the TMF life with increasing nitrogen. Thus, the nitrogen content played an important role in controlling the dynamics of planar slip that governs the cyclic deformation and life under TMF. In case of IF tests, the slip mode was observed to be wavy, mixed, and planar, respectively, at the nitrogen contents of 0.07, 0.14, and 0.22 wt pct. A mixed mode of deformation seen at the intermediate nitrogen content of 0.14 wt pct (Figures 3(c) and (d)) appears to have caused a peak in IF life therein, compared to the other two heats.

In addition to the above, nitrogen content is also observed to influence the development of mean stress during TMF cycling, as seen from Figure 1(d). With reference to the above figure, it can be noted that a reduction in the nitrogen content led to an increase in the compressive mean stress under IP-TMF and a decrease in the tensile mean stress under OP-TMF. As mentioned before, the severity of intergranular cracking in IP-TMF is directly related to the peak tensile stress. A reduction in the nitrogen content thus seems potentially beneficial in improving the life under TMF cycling. The mechanistic role of nitrogen content on the development of mean stress could not be understood from the present studies. However, this seems to lie in the differences in manifestations of DSA during tensile and compressive regimes of hysteresis loop, which needs further investigations that are beyond the scope of the present study.

The above investigations revealed that IF cycling at the T_{\max} of expected thermal cycle does not always provide conservative life estimation for the component under actual service. Similar results have been reported in other materials as well, with the life variations being sensitive to the material, environment, and the applied strain range.^[1–3,14,22,42] These observations call for a modification in the safety factors used in the generation of fatigue design curves, to account for temporal dependence of cyclic deformation on temperature and strain.

IV. SUMMARY

1. Dynamic strain aging played a decisive role in defining cyclic lives under TMF deformation of type 316LN stainless steel, particularly for high nitrogen contents (0.14 and 0.22 wt pct N). However, both DSA and recovery processes are observed to be significant under isothermal cycling.
2. Dislocation substructures are found to depend both on the nitrogen content and the type of test. Extensive slip localization is observed in TMF, as reflected by an increase in the density of planar slip bands with an increase in the nitrogen content. Planar slip due to both DSA and nitrogen content is found to be more predominant at 0.22 wt pct N.
3. Out-of-phase TMF cycling (OP-TMF) consistently yielded higher lives compared to both in-phase

TMF (IP-TMF) and IF at the peak temperature. In-phase cycling proved most deleterious by imparting a greater intergranular damage compared to OP-TMF and IF cycling. It is important to mention that the order sequence of fatigue life (*i.e.*, IP-TMF < IF < OP-TMF) remained same, irrespective of the nitrogen content in 316LN SS.

- In IP and OP-TMF cycling, increasing nitrogen content promoted strong slip localization in combination with high tensile cyclic stresses that marred the beneficial effect of nitrogen on TMF life, and thus 316LN SS with 0.07 wt pct N showed the maximum in TMF life. However, the intermediate nitrogen content of 0.14 wt pct showed a slight improvement in life over the other two steels under IF cycling.

ACKNOWLEDGMENTS

Authors would like to thank Mr. M. Srinivasa Rao, IGCAR, Kalpakkam, Mrs. D. Kanchanamala, and Mr. M. Papa Rao, IIT Madras for their assistance in testing, TEM sample preparation and examination.

REFERENCES

- M. Fujino and S. Taira: *Proc. ICM* 3, 1979, vol. 2, pp. 49–58.
- E.G. Ellison and A. Al-Zamily: *Fatigue Fract. Eng. Mater. Struct.*, 1994, vol. 17 (1), pp. 39–51.
- S.Y. Zamrik, D.C. Davis, and L.C. Firth: in *Thermomechanical Fatigue Behaviour of Materials, ASTM STP 1263*, M.J. Verrilli and M.G. Castelli, eds., ASTM, Philadelphia, 1996, pp. 96–116.
- M. Ramesh, H.J. Leber, K.G.F. Janssens, M. Diener, and R. Spolenak: *Int. J. Fatigue*, 2011, vol. 33, pp. 683–91.
- S. Degallaix, J.I. Dickson, and J. Foct: in *Proc. Int. Conf. on High Nitrogen Steels, HNS'88*, J. Foct, and A. Hendry, eds., Lille, France, 1989, pp. 380–86.
- D.W. Kim, W.-S. Ryu, J.H. Hong, and S.-K. Choi: *J. Nucl. Mater.*, 1998, vol. 254, pp. 226–33.
- G.V. Prasad Reddy, R. Sandhya, S. Sankaran, and M.D. Mathew: *Metall. Mater. Trans. A*, 2014, vol. 45A, pp. 5057–67.
- D.W. Kim, C.H. Han, and W.-S. Ryu: *Mater. Sci. Forum*, 2005, vols. 475–479, pp. 1429–32.
- K. Oda, N. Kondo, and K. Shibata: *ISIJ Int.*, 1990, vol. 30 (8), pp. 625–31.
- G.V. Prasad Reddy, R. Sandhya, S. Sankaran, and M.D. Mathew: *Metall. Mater. Trans. A*, 2014, vol. 45A, pp. 5044–56.
- V.S. Srinivasan, R. Sandhya, M. Valsan, K.B.S. Rao, S.L. Mannan, and D.H. Sastry: *Scripta Mater.*, 1997, vol. 37 (10), pp. 1593–98.
- G.V. Prasad Reddy, R. Sandhya, K.B.S. Rao, and S. Sankaran: *Proc. Eng.*, 2010, vol. 2, pp. 2181–88.
- M.S. Pham and S.R. Holdsworth: *Int. J. Fatigue*, 2013, vol. 51, pp. 36–48.
- A. Nagesha, M. Valsan, R. Kannan, K. Bhanu Sankara Rao, V. Bauer, H.J. Christ, and V. Singh: *Int. J. Fatigue*, 2009, vol. 31, pp. 636–43.
- M.S. Pham and S.R. Holdsworth: *Mater. Sci. Eng. A*, 2012, vol. 556, pp. 122–33.
- M.S. Pham and S.R. Holdsworth: *Metall. Mater. Trans. A*, 2014, vol. 45A, pp. 738–51.
- M. Ivanchenko: Ph.D. Thesis, Aalto University, Espoo, Finland, 2010.
- J.D. Baird: in *The inhomogeneities of Plastic Deformation*, R.E. Reed-Hill, ed., American Society for Metals, Metals Park, OH, 1973, p. 191–222.
- E. Pink and A. Grinberg: *Mater. Sci. Eng.*, 1981, vol. 571, pp. 1–8.
- M.L.G. Byrnes, M. Grujicic, and W.S. Owen: *Acta Metall.*, 1987, vol. 35 (7), pp. 1853–62.
- H.J. Frost and M.F. Ashby: *Deformation-Mechanism Maps*, Pergamon Press, Oxford, 1982.
- R. Zauter, F. Petry, H.J. Christ, and H. Mugarabi: in *Thermo-mechanical Fatigue Behavior of Materials, ASTM STP 1189*, H. Sehitoglu, ed., ASTM, Philadelphia, 1993, pp. 70–90.
- S. Taira and M. Fujino: *J. Soc. Met. Sci. Jpn.*, 1976, vol. 25, pp. 375–81.
- M. Gerland, J. Mendez, J. Lepinoux, and P. Violan: *Mater. Sci. Eng. A*, 1993, vol. 164, pp. 226–29.
- M. Gerland, R. Alain, B. Ait Saadi, and J. Mendez: *Mater. Sci. Eng. A*, 1997, vol. 229, pp. 68–86.
- B. Weiss and R. Stickler: *Metall. Trans.*, 1972, vol. 3, pp. 851–66.
- M. Deighton: *J. Iron Steel Inst.*, 1970, vol. 208, pp. 1012–20.
- A.F. Padilha, D.M. Escriba, E. Materna-Morris, M. Rieth, and M. Klimenkov: *J. Nucl. Mater.*, 2007, vol. 362, pp. 132–38.
- G. Pecker and I.M. Bernstein: *Handbook of Stainless Steels*, McGraw-Hill, New York, 1977.
- G. Wahlberg, U. Rolander, and H.O. Andren: in *Proc. Int. Conf. on High Nitrogen Steels, HNS'88*, J. Foct, A. Hendry, eds., Lille, France, 1989, pp. 163–68.
- T.H. Lee, S.J. Kim, and Y.C. Jung: *Metall. Mater. Trans. A*, 2000, vol. 31A, pp. 1713–23.
- M. Kikuchi, M. Kajihara, and S.K. Choi: *Mater. Sci. Eng. A*, 1991, vol. 146 (1–2), pp. 131–50.
- P. Shankar, D. Sundararaman, and S. Ranganathan: *Scripta Metall. Mater.*, 1994, vol. 31 (5), pp. 589–93.
- S. Taira, M. Fujino, and R. Ohtani: *Fatigue Eng. Mater. Struct.*, 1979, vol. 1, pp. 495–508.
- A.N. Stroh: *Proc. R. Soc. Lond. A*, 1955, vol. 232, p. 548.
- D. McLean: *Grain Boundaries in Metals*, Clarendon Press, Oxford, U.K., 1957.
- C. Gandhi and R. Raj: *Metall. Trans. A*, 1981, vol. 12A, pp. 515–20.
- K. Yagi, C. Tanaka, K. Kubo, and O.U. Kanemar: *ISIJ Int.*, 1985, vol. 25, pp. 1179–86.
- M.W. Spindler: *Mater. Sci. Technol.*, 2007, vol. 23 (12), pp. 1461–70.
- E.G. Ellison and A.J.F. Paterson: in *Proceedings, Institution of Mechanical Engineers*, 1976, vol. 190, p. 319–30.
- P. Rodriguez and K. Bhanu Sankara Rao: *Prog. Mater. Sci.*, 1993, vol. 37, pp. 403–80.
- A. Nagesha, R. Kannan, G.V.S. Sastry, R. Sandhya, V. Singh, K. Bhanu Sankara Rao, and M.D. Mathew: *Mater. Sci. Eng. A*, 2012, vol. 554, pp. 95–104.
- M. Valsan, D.H. Sastry, K.B.S. Rao, and S.L. Mannan: *Metall. Mater. Trans. A*, 1994, vol. 25A, pp. 159–71.
- M.D. Mathew, K. Laha, and V. Ganesan: *Mater. Sci. Eng. A*, 2012, vol. 535, pp. 76–83.